Results in Physics 60 (2024) 107632

Contents lists available at ScienceDirect

Results in Physics

journal homepage: www.elsevier.com/locate/rinp

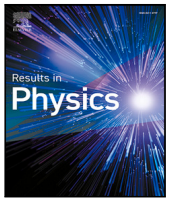

Optimal tripartite quantum teleportation protocols via noisy channels by feed-forward control and environment-assisted measurement

Peiyao Zhang [a], Xiujuan Lu [b], Sen Kuang [a,*], Daoyi Dong [c]

[a] Department of Automation, University of Science and Technology of China, Hefei 230027, China
[b] Department of Mechanical Engineering, The University of Hong Kong, 999077, Hong Kong, China
[c] School of Engineering, Australian National University, Canberra, ACT 2601, Australia

ARTICLE INFO

Keywords:
Environment-assisted measurement
Feed-forward control
Tripartite teleportation
Weak measurement

ABSTRACT

This paper presents a tripartite quantum teleportation protocol that incorporates feed-forward control and environment-assisted measurement, aiming to suppress the influence of arbitrary noise with at least one reversible Kraus operator. In this protocol, the feed-forward control is first utilized before the decoherence channel, such that the entangled qubit is transferred to the target state, which is more robust against noise. Next, the measurement is performed on the noise environment coupled with the entangled qubit during the decoherence channel. Finally, the reversed feed-forward control and the redesigned weak measurement reversal operator are applied after the decoherence channel. This protocol can be applied to the case where both amplitude damping and phase damping noise coexist. Based on this protocol, the analytical expressions for performance metrics including the average fidelity and the success probability are further derived. Even for the heavy damping cases, the final average teleportation fidelity can reach 1, which is independent of the magnitude of decoherence and the entanglement parameters. Furthermore, we optimize the success probability without compromising fidelity, and derive the average fidelity expression of the standard tripartite teleportation protocol through the phase damping noise channel. The effectiveness of our protocol is verified by numerical simulations.

Introduction

Quantum teleportation is one of the most essential protocols in quantum information technology, which can overcome the distance limitation of direct quantum state transfer and achieve nonlocal transmission of an unknown quantum state. Significant progress has been made in using quantum teleportation to construct the quantum communication network [1–3], and typical teleportation schemes include controlled teleportation [4–6], bidirectional teleportation [7,8], cyclic teleportation [9,10], quantum repeater [11,12], and tripartite teleportation [13,14]. While most of these schemes have developed significantly in both theory and experiments, tripartite teleportation is worth further investigating. The tripartite teleportation is a quantum information transmission protocol, where the sender uses a tripartite entangled state to transmit an unknown state to either of the two receivers. In this process, successful teleportation relies on the prior entanglement distribution and quantum channel construction. However, the entanglement distribution process will inevitably be affected by environmental noise, leading to decoherence in the entangled states and thereby degrading the quantum channel. Hence, developing practical teleportation protocols that mitigate the effects of decoherence has become a focal point and challenge.

Amplitude damping (AD) and phase damping (PD) are two typical decoherence mechanisms [15–17]. The amplitude damping channel (ADC) dissipates the energy of the quantum system into the environment, leading to decay towards a temperature-related steady state (e.g., spontaneous emission of photons from atoms). The phase damping channel (PDC) introduces random displacements of quantum states, causing partial loss of phase information. To mitigate the effects of AD and PD on quantum channels and improve the fidelity of quantum teleportation, two major categories of methods have been proposed. The first category focuses on restoring entangled states from noise effect, and various related techniques have been proposed, including quantum error correction [18,19], entanglement distillation [20,21], and dynamical decoupling [22]. Although these schemes can improve the fidelity of quantum teleportation, the final performance is limited to the magnitude of decoherence, entanglement parameters, and redundant auxiliary qubits. The second category involves modifying the

* Corresponding author.
E-mail address: skuang@ustc.edu.cn (S. Kuang).

https://doi.org/10.1016/j.rinp.2024.107632
Received 13 March 2024; Accepted 30 March 2024
Available online 8 April 2024

teleportation protocol to adapt to the noisy quantum channel, which is based on applying redesigned reversed operators to replace unitary operations in the last step [23–25]. Compared with the first category method, the second category protocol offers clear advantages, which just need a single copy of an entangled state, and can always achieve optimal quantum teleportation (i.e., maximizing the success probability for the given fidelity).

In addition to the above methods, the weak measurement (WM) is also used to suppress decoherence, which has been found wide applications in both theory and experiments [26,27]. As an extension of the traditional von Neumann orthogonal projective measurement, WM reduces disturbance on the system by weakening the measurement interaction to prevent the quantum state from collapsing into one of its eigenstates after measurement. In quantum WM, there is a trade-off between the obtained information and the system disturbance, i.e., higher measurement strengths offer more information while simultaneously causing increased system disturbance. Based on the development of WM, various decoherence suppression strategies are proposed, including quantum feedback control (QFBC) [28,29], quantum measurement reversal (QMR) [23,30], and quantum feed-forward control (QFFC) [31,32]. The QFBC involves extracting information from the quantum state after passing through the decoherence channel. In the QFBC, it requires prior knowledge of the initial entanglement parameters and is challenging to achieve sufficiently high fidelity. In contrast, the QMR does not require prior information about the initial state. The QMR involves applying WM to the qubit before the decoherence channel to reduce the weight of excited states, and designing the weak measurement reversal (WMR) operator after the decoherence channel to approximately restore the state to its initial state. The QFFC builds upon the QMR by adding feed-forward control operators and feed-forward control reversal operators. This allows the transfer of qubits to the desired target states that are more robust against noise, resulting in the more effective suppression of decoherence. Note that the methods based on WM mentioned above are operating on the controlled quantum system. There are also several approaches to suppress decoherence by manipulating the environment coupled to the quantum system, such as environment-assisted error correction (EAEC) [33] and environment-assisted measurement (EAM) [34]. The EAEC involves measuring the noise environment coupled to the controlled system and designing a reversal operator based on the measurement results to recover the input state. This method can recover the unknown quantum state coupled to the noise environment with a constant success probability of 1. However, it has significant limitations, primarily requiring the evolution of the quantum system to have a random unitary Kraus decomposition, which rarely exists in a generic dissipative model. Based on the EAEC, the EAM was proposed in [34], which offers broader applicability and higher fidelity as it can be employed in any noise environment that contains at least one reversible Kraus operator.

Currently, existing quantum teleportation protocols for suppressing decoherence are only applicable to specific forms of decoherence channels [23,35–37], which involve redesigning specific forms of reversed operators. However, in practical environments, there exists a wide variety of noise sources with different characteristics. Moreover, these protocols are affected by control parameters, the magnitude of decoherence, and entanglement parameters, making it challenging to achieve satisfactory fidelity under heavy damping conditions. To tackle these challenges, we propose a tripartite quantum teleportation protocol that combines QFFC and EAM (FF-EM). This protocol utilizes feed-forward control before the decoherence channel, employs EAM during the decoherence channel, and applies feed-forward reversal after decoherence. In the last step, we use a redesigned WMR operator instead of a unitary operation to counteract the effects of the noise channel. Based on our protocol, we derive the expression for the final success probability, and provide the optimal success probability and its corresponding optimal conditions. Compared with the aforementioned protocols, our protocol has the capability to handle decoherence channels with both amplitude and phase damping noise simultaneously. This is a significant improvement as it addresses a wider range of noise types commonly encountered in practical environments. Furthermore, our protocol is designed to maintain a fidelity of 1 regardless of the magnitude of decoherence and entanglement parameters. In addition, our scheme significantly improves the success probability compared to the EA-WMR quantum teleportation protocol proposed in [35]. Specifically, we provide the standard tripartite teleportation protocol with two qubits passing through PDC, and derive the expressions for performance metrics.

The paper is structured as follows. In Section "Standard tripartite teleportation protocol", we introduce the processes of the standard tripartite quantum teleportation protocol in the presence of phase damping noise, and derive the average teleportation fidelity. In Section "Tripartite quantum teleportation protocol with feed-forward control and environment-assisted measurement", we propose the FF-EM tripartite quantum teleportation protocol and calculate the success probability and the average teleportation fidelity. Finally, Section "Conclusion" provides the conclusion.

Standard tripartite teleportation protocol

This section takes the analysis of ADC and PDC as examples to introduce the critical details of the standard tripartite teleportation protocol. It serves as a basis for discussing the problems to be solved in this paper.

The effect of AD on a single qubit can be denoted as $|0\rangle_S|0\rangle_E \xrightarrow{e_0,e_1} |0\rangle_S|0\rangle_E$ or $|1\rangle_S|0\rangle_E \xrightarrow{e_0,e_1} \sqrt{1-r}|1\rangle_S|0\rangle_E + \sqrt{r}|0\rangle_S|1\rangle_E$, $(r = 1 - e^{\Gamma t})$. Here $r \in [0,1]$ is the magnitude of decoherence, Γ is the energy relaxation rate, the subscripts "S" and "E" denote the quantum system and its environment, respectively, and e_0 and e_1 are Kraus operators defined as [15]

$$e_0 = |0\rangle\langle 0| + \sqrt{1-r}|1\rangle\langle 1|,\ e_1 = \sqrt{r}|0\rangle\langle 1|. \tag{1}$$

In this paper, assume that r is known and the noise can be fully characterized.

The noise does not affect atoms in the ground state $|0\rangle_S$, but for atoms in the excited state $|1\rangle_S$, it causes them to decay to the ground state $|0\rangle_S$ and emit photons into the surrounding environment. Thus, it is possible to determine whether decoherence is occurring by EAM, which will be used in Section "Tripartite quantum teleportation protocol with feed-forward control and environment-assisted measurement" to mitigate the effects of noise.

More details about performance metrics of the standard tripartite teleportation protocol under AD have already been provided in [35]. Below, we outline the standard tripartite teleportation protocol under PD.

The effect of PD on a single qubit density matrix ρ can be expressed as $\varepsilon_r(\rho) = rZ\rho Z + (1-r)\rho$, where Z is the Pauli matrix σ_z. This indicates that PD noise has a probability of $(1-r)$ preserving the system state and a probability of r inducing a phase flip along the direction of Z. The corresponding Kraus operators are defined as [15]

$$e_0 = |0\rangle\langle 0| + \sqrt{1-r}|1\rangle\langle 1|,\ e_1 = \sqrt{r}|1\rangle\langle 1|. \tag{2}$$

In tripartite quantum teleportation, Alice is the sender and possesses the unknown qubit 0 to be transmitted, as well as a tripartite entangled state $|\psi\rangle_{123}$, while Bob and Charlie are the receivers. Receivers assist each other in the quantum channel to jointly reconstruct qubit 0 at either receiver's location. For example, consider the case of reconstructing qubit 0 at Charlie's location here. Let qubit 0 be the input state, which is defined as

$$\rho_{in} = |\psi_0\rangle\langle\psi_0|,\ |\psi_0\rangle = \alpha|0\rangle + \beta|1\rangle, \tag{3}$$

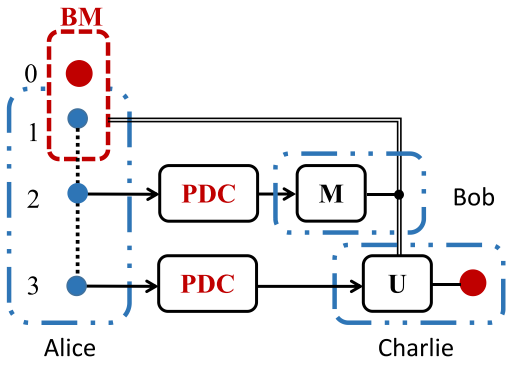

Fig. 1. Standard tripartite quantum teleportation protocol through PDC. The dashed lines in the figure indicate quantum entanglement, the double lines indicate the classical channels, the single lines indicate quantum channels, BM denotes Bell basis measurement, M denotes the quantum measurement, and U denotes the unitary operation.

where $|\alpha|^2 + |\beta|^2 = 1$. The tripartite entangled state prepared by Alice can be expressed as (using GHZ state as an example)

$$|\psi_{123}\rangle = \cos\frac{\theta}{2}|000\rangle + \sin\frac{\theta}{2}|111\rangle, \tag{4}$$

where $0 \leqslant \theta \leqslant \pi/2$. When $\theta = \pi/2$, it corresponds to the maximum entangled state.

The protocol process is depicted in Fig. 1, which includes the following three steps.

Step 1 Alice employs entanglement distribution through PDC, thereby constructing a quantum channel, sending qubits 2 and 3 to Bob and Charlie, respectively.

Qubits 2 and 3 enter the noise channel. Then, the three-qubit Kraus operators for the GHZ entangled state can be expressed as

$$\begin{aligned} &E_{00} = I \otimes e_0 \otimes e_0,\ E_{01} = I \otimes e_0 \otimes e_1,\\ &E_{10} = I \otimes e_1 \otimes e_0,\ E_{11} = I \otimes e_1 \otimes e_1, \end{aligned} \tag{5}$$

where e_0 and e_1 are given by Eq. (2), and I is the identity operator.

After passing through the noise channel, the entangled state $|\psi_{123}\rangle$ under the action of the Kraus operator becomes

$$\begin{aligned} &|\psi_{123}^{E_{ij}}\rangle = E_{ij}|\psi_{123}\rangle,\ (i,j=0,1),\\ &|\psi_{123}^{E_{00}}\rangle = \cos\frac{\theta}{2}|000\rangle + (1-r)\sin\frac{\theta}{2}|111\rangle,\\ &|\psi_{123}^{E_{01}}\rangle = |\psi_{123}^{E_{10}}\rangle = \sqrt{r(1-r)}\sin\frac{\theta}{2}|111\rangle,\\ &|\psi_{123}^{E_{11}}\rangle = r\sin\frac{\theta}{2}|111\rangle. \end{aligned} \tag{6}$$

Step 2 Alice applies a Bell joint measurement on the input qubit 0 and her entangled qubit 1, and Bob measures his entangled qubit 2.

The teleportation process of $|\psi_{123}^{E_{00}}\rangle$ is given below, and the analysis of the remaining cases can be obtained similarly. The quantum state of the whole system can be described by

$$|\psi_S^{E_{00}}\rangle = (\alpha|0\rangle + \beta|1\rangle)_0 \otimes \left(\cos\frac{\theta}{2}|000\rangle + (1-r)\sin\frac{\theta}{2}|111\rangle\right)_{123}. \tag{7}$$

Alice performs Bell joint measurement on qubits 0 and 1. After applying the CNOT gate on qubit 1 (target qubit) in the entangled state and qubit 0 (control qubit), subsequently applying H gate to the qubit 0, the quantum state of the whole system can be obtained as

$$\begin{aligned} &|\psi_S^{E_{00}}\rangle^{BM}\\ &= \frac{1}{\sqrt{2}}|00\rangle_{01}\left(\alpha\cos\frac{\theta}{2}|00\rangle + \beta(1-r)\sin\frac{\theta}{2}|11\rangle\right)_{23}\\ &\quad + \frac{1}{\sqrt{2}}|01\rangle_{01}\left(\beta\cos\frac{\theta}{2}|00\rangle + \alpha(1-r)\sin\frac{\theta}{2}|11\rangle\right)_{23}\\ &\quad + \frac{1}{\sqrt{2}}|10\rangle_{01}\left(\alpha\cos\frac{\theta}{2}|00\rangle - \beta(1-r)\sin\frac{\theta}{2}|11\rangle\right)_{23}\\ &\quad + \frac{1}{\sqrt{2}}|11\rangle_{01}\left(-\beta\cos\frac{\theta}{2}|00\rangle + \alpha(1-r)\sin\frac{\theta}{2}|11\rangle\right)_{23}. \end{aligned} \tag{8}$$

Bob performs a projective measurement on his qubit 2, using the measurement basis

$$\begin{aligned} &|0\rangle_2 = \sin\frac{\varphi}{2}|x_0\rangle_2 + \cos\frac{\varphi}{2}|x_1\rangle_2,\\ &|1\rangle_2 = \cos\frac{\varphi}{2}|x_0\rangle_2 - \sin\frac{\varphi}{2}|x_1\rangle_2. \end{aligned} \tag{9}$$

If the Bell joint measurement results of qubits 0 and 1 are $(0,0)$, then the state of qubits 2 and 3 becomes

$$\begin{aligned} &|\eta_{00}^{E_{00}}\rangle_{23}^{M}\\ &= \frac{1}{\sqrt{2}}|x_0\rangle_2\left(\alpha\cos\frac{\theta}{2}\sin\frac{\varphi}{2}|0\rangle + \beta(1-r)\sin\frac{\theta}{2}\cos\frac{\varphi}{2}|1\rangle\right)_3\\ &\quad + \frac{1}{\sqrt{2}}|x_1\rangle_2\left(\alpha\cos\frac{\theta}{2}\cos\frac{\varphi}{2}|0\rangle - \beta(1-r)\sin\frac{\theta}{2}\sin\frac{\varphi}{2}|1\rangle\right)_3. \end{aligned} \tag{10}$$

Therefore, the state of the corresponding qubit 3 can be obtained based on the measurement result of the qubit 2. Using a similar approach for other cases, the final state of the qubit 3 held by Charlie after two measurements can be obtained for all Kraus operators, as shown in Table 1.

Step 3 Alice and Bob transmit the two measurement results to Charlie through the classical channel. Based on the measurement results of qubits 0, 1, and 2, Charlie applies the corresponding unitary operator in Table 1 to the qubit 3. Then the final output quantum state is obtained as

$$\rho_{m,n,k}^{out} = \sum_{i,j=0,1} U_{m,n,k}\rho_{m,n,k}^{E_{ij}}U_{m,n,k}^{\dagger}, \tag{11}$$

where $U_{m,n,k}$ is the chosen unitary operator, and $\rho_{m,n,k}^{E_{ij}}$ is the density operator for qubit 3 with the Kraus operator E_{ij} and the measurement results (m,n,k).

After introducing the process of the standard teleportation (the case of ADC can be referred to [35]), next, we focus on its evaluation index of effectiveness. Here, we select the average fidelity as the evaluation index, i.e.,

$$\mathrm{Fid}_{\mathrm{av}} = \int \mathrm{d}\psi \sum_{m,n,k} p_{m,n,k}\,\mathrm{fid}_{m,n,k}, \tag{12}$$

where $\mathrm{fid}_{m,n,k} = \langle\psi_0|\rho_{m,n,k}^{out}|\psi_0\rangle$ is the fidelity for the measurement results (m,n,k), representing the difference between the final output state and the input state, and $p_{m,n,k} = \mathrm{Tr}\left(\sum_{i,j}\rho_{m,n,k}^{E_{ij}}\right)$ is the probability for the measurement results (m,n,k). Note that the average fidelity $\mathrm{Fid}_{\mathrm{av}}$ mentioned here is a general metric that applies to both the cases of ADC and PDC.

According to Eq. (12) the average standard teleportation fidelity through PDC is calculated as

$$\mathrm{Fid}_{\mathrm{av}}^{\mathrm{pd}} = \frac{1}{3}\sin\varphi\sin\theta(1-r) + \frac{2}{3} \tag{13}$$

and the average standard teleportation fidelity through ADC given in [35] is

$$\mathrm{Fid}_{\mathrm{av}}^{\mathrm{ad}} = \frac{1}{2}(1-\cos\theta)\left(\frac{r^2}{3} - \frac{r}{2}\right) + \frac{1}{3}\sin\varphi\sin\theta(1-r) + \frac{2}{3}, \tag{14}$$

where r is the magnitude of decoherence defined in Eq. (1), θ is the entanglement parameter given in Eq. (4), and φ is the measurement parameter on qubit 2 defined in Eq. (9).

Table 1
Charlie's states $|\psi_{mnk}^{EM_{ij}}\rangle$ corresponding to the measurement results of Alice and Bob (m,n,k).

$(m,n,k)_{012}$	$\|\psi_{mnk}^{EM_{00}}\rangle_3$	$\|\psi_{mnk}^{EM_{01,10}}\rangle_3$	$\|\psi_{mnk}^{EM_{11}}\rangle_3$	U
(0, 0, 0)	$\frac{1}{\sqrt{2}}\left(\alpha\cos\frac{\theta}{2}\sin\frac{\varphi}{2}\|0\rangle_3+\beta(1-r)\sin\frac{\theta}{2}\cos\frac{\varphi}{2}\|1\rangle_3\right)$	$\frac{1}{\sqrt{2}}\beta\sqrt{r(1-r)}\sin\frac{\theta}{2}\cos\frac{\varphi}{2}\|1\rangle_3$	$\frac{1}{\sqrt{2}}\beta r\sin\frac{\theta}{2}\cos\frac{\varphi}{2}\|1\rangle_3$	I
(0, 0, 1)	$\frac{1}{\sqrt{2}}\left(\alpha\cos\frac{\theta}{2}\cos\frac{\varphi}{2}\|0\rangle_3-\beta(1-r)\sin\frac{\theta}{2}\sin\frac{\varphi}{2}\|1\rangle_3\right)$	$-\frac{1}{\sqrt{2}}\beta\sqrt{r(1-r)}\sin\frac{\theta}{2}\sin\frac{\varphi}{2}\|1\rangle_3$	$-\frac{1}{\sqrt{2}}\beta r\sin\frac{\theta}{2}\sin\frac{\varphi}{2}\|1\rangle_3$	σ_z
(0, 1, 0)	$\frac{1}{\sqrt{2}}\left(\beta\cos\frac{\theta}{2}\sin\frac{\varphi}{2}\|0\rangle_3+\alpha(1-r)\sin\frac{\theta}{2}\cos\frac{\varphi}{2}\|1\rangle_3\right)$	$\frac{1}{\sqrt{2}}\alpha\sqrt{r(1-r)}\sin\frac{\theta}{2}\cos\frac{\varphi}{2}\|1\rangle_3$	$\frac{1}{\sqrt{2}}\alpha r\sin\frac{\theta}{2}\cos\frac{\varphi}{2}\|1\rangle_3$	σ_x
(0, 1, 1)	$\frac{1}{\sqrt{2}}\left(\beta\cos\frac{\theta}{2}\cos\frac{\varphi}{2}\|0\rangle_3-\alpha(1-r)\sin\frac{\theta}{2}\sin\frac{\varphi}{2}\|1\rangle_3\right)$	$-\frac{1}{\sqrt{2}}\alpha\sqrt{r(1-r)}\sin\frac{\theta}{2}\sin\frac{\varphi}{2}\|1\rangle_3$	$-\frac{1}{\sqrt{2}}\alpha r\sin\frac{\theta}{2}\sin\frac{\varphi}{2}\|1\rangle_3$	$\sigma_x\sigma_z$
(1, 0, 0)	$\frac{1}{\sqrt{2}}\left(\alpha\cos\frac{\theta}{2}\sin\frac{\varphi}{2}\|0\rangle_3-\beta(1-r)\sin\frac{\theta}{2}\cos\frac{\varphi}{2}\|1\rangle_3\right)$	$-\frac{1}{\sqrt{2}}\beta\sqrt{r(1-r)}\sin\frac{\theta}{2}\cos\frac{\varphi}{2}\|1\rangle_3$	$-\frac{1}{\sqrt{2}}\beta r\sin\frac{\theta}{2}\cos\frac{\varphi}{2}\|1\rangle_3$	σ_z
(1, 0, 1)	$\frac{1}{\sqrt{2}}\left(\alpha\cos\frac{\theta}{2}\cos\frac{\varphi}{2}\|0\rangle_3+\beta(1-r)\sin\frac{\theta}{2}\sin\frac{\varphi}{2}\|1\rangle_3\right)$	$\frac{1}{\sqrt{2}}\beta\sqrt{r(1-r)}\sin\frac{\theta}{2}\sin\frac{\varphi}{2}\|1\rangle_3$	$\frac{1}{\sqrt{2}}\beta r\sin\frac{\theta}{2}\sin\frac{\varphi}{2}\|1\rangle_3$	I
(1, 1, 0)	$\frac{1}{\sqrt{2}}\left(-\beta\cos\frac{\theta}{2}\sin\frac{\varphi}{2}\|0\rangle_3+\alpha(1-r)\sin\frac{\theta}{2}\cos\frac{\varphi}{2}\|1\rangle_3\right)$	$\frac{1}{\sqrt{2}}\alpha\sqrt{r(1-r)}\sin\frac{\theta}{2}\cos\frac{\varphi}{2}\|1\rangle_3$	$\frac{1}{\sqrt{2}}\alpha r\sin\frac{\theta}{2}\cos\frac{\varphi}{2}\|1\rangle_3$	$\sigma_z\sigma_x$
(1, 1, 1)	$\frac{1}{\sqrt{2}}\left(-\beta\cos\frac{\theta}{2}\cos\frac{\varphi}{2}\|0\rangle_3-\alpha(1-r)\sin\frac{\theta}{2}\sin\frac{\varphi}{2}\|1\rangle_3\right)$	$-\frac{1}{\sqrt{2}}\alpha\sqrt{r(1-r)}\sin\frac{\theta}{2}\sin\frac{\varphi}{2}\|1\rangle_3$	$-\frac{1}{\sqrt{2}}\alpha r\sin\frac{\theta}{2}\sin\frac{\varphi}{2}\|1\rangle_3$	σ_x

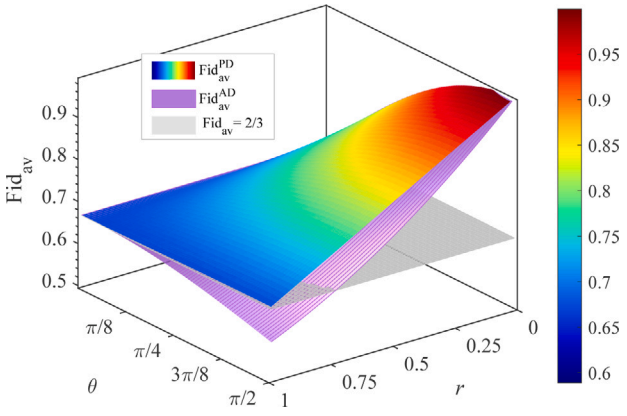

Fig. 2. Average standard tripartite teleportation fidelities through PDC and ADC.

Combined with Eqs. (13) and (14), it is seen that the average teleportation fidelities both take the maximum value when $\varphi = \pi/2$. Fig. 2 shows the optimal average fidelities for these two types of noises, and it can be seen that with the increase in the magnitude of decoherence r and the decrease in the entanglement parameter θ, the average teleportation fidelities through ADC and PDC both decrease. Even at maximum entanglement ($\theta = \pi/2$), the average teleportation fidelity through ADC is still lower than the classical limit 2/3. When both AD and PD noises are present, the average teleportation fidelity will be more seriously affected.

To solve the problem of fidelity degradation caused by noise, we propose a tripartite quantum teleportation protocol assisted by feed-forward control and environment-assisted measurement (FF-EM). In this protocol, the fidelity will be not limited by the magnitude of decoherence and the entanglement parameter (remaining constantly at 1). Unlike most teleportation protocols for suppressing decoherence that are only applicable to one specific form of noise, the FF-EM protocol is suitable for scenarios where both AD and PD coexist, as will be highlighted in the next section.

Tripartite quantum teleportation protocol with feed-forward control and environment-assisted measurement

In this section, the FF-EM tripartite quantum teleportation protocol is proposed based on the standard teleportation protocol. The fundamental idea behind this protocol is as follows. Before the noise channel, we employ the WM and feed-forward control operators. During the noise channel, we utilize EAM. After the noise channel, we apply feed-forward reversal operators. And instead of using unitary operations, in the final step of the protocol, we utilize WMR operators to restore the input state.

The protocol process is depicted in Fig. 3, which includes the following three steps.

Step 1 Alice sends qubits 2 and 3 to Bob and Charlie, respectively, through the noise channel. Unlike the standard quantum teleportation protocol proposed in Section "Standard Tripartite Teleportation Protocol", the FF-EM protocol presented here introduces extra steps involving pre-WM, EAM, and feed-forward control and reversal.

Below we will introduce the detailed procedures.

- Pre-WM

To obtain more information about the quantum state, the complete pre-WM operators m_0 and m_1 are, respectively, applied to the entangled qubits 2 and 3 distributed by Alice before the decoherence channel. Then we have $\Pi_{i=0,1} m_i^\dagger m_i = [I + \cos(\omega) Z]/2$, $\Sigma_{i=0,1} m_i^\dagger m_i = I$, where Z is the Pauli matrix σ_z. We define m_0 and m_1 along the z axis as

$$m_0 = \begin{bmatrix} \cos(\omega/2) & 0 \\ 0 & \sin(\omega/2) \end{bmatrix}, \; m_1 = \begin{bmatrix} \sin(\omega/2) & 0 \\ 0 & \cos(\omega/2) \end{bmatrix}, \tag{15}$$

where $0 \leqslant \omega \leqslant \pi/2$ depends on the measurement strength. When $\omega = \pi/2$, the measurement does not affect the system. When $\omega = 0$, the measurement strength is the strongest and it is equivalent to a projective measurement. When $0 < \omega < \pi/2$, the measurement is considered as a WM, which balances the information gain and the interference on the system.

There is no operation on the qubit 1 and WMs are used for qubits 2 and 3. The Pre-WM operators for qubits 1, 2 and 3 are

$$\begin{aligned} &M_{00} = I \otimes m_0 \otimes m_0, \; M_{01} = I \otimes m_0 \otimes m_1, \\ &M_{10} = I \otimes m_1 \otimes m_0, \; M_{11} = I \otimes m_1 \otimes m_1. \end{aligned} \tag{16}$$

After employing the WM, the probability of the tripartite entangled state $|\psi_{123}\rangle$ in Eq. (6) transitioning to $|\psi_{M_{ij}}\rangle$ is

$$g_{M_{ij}} = \mathrm{Tr}\left(M_{ij}|\psi_{123}\rangle\langle\psi_{123}|M_{ij}^\dagger\right), \; \sum_{i,j=0,1} g_{M_{ij}} = 1, \tag{17}$$

where

$$\begin{aligned} |\psi_{M_{00}}\rangle &= \cos\frac{\theta}{2}\cos^2\frac{\omega}{2}|000\rangle + \sin\frac{\theta}{2}\sin^2\frac{\omega}{2}|111\rangle, \\ |\psi_{M_{01}}\rangle &= |\psi_{M_{10}}\rangle = \cos\frac{\theta}{2}\sin\frac{\omega}{2}\cos\frac{\omega}{2}|000\rangle \\ &\quad + \sin\frac{\theta}{2}\sin\frac{\omega}{2}\cos\frac{\omega}{2}|111\rangle, \\ |\psi_{M_{11}}\rangle &= \cos\frac{\theta}{2}\sin^2\frac{\omega}{2}|000\rangle + \sin\frac{\theta}{2}\cos^2\frac{\omega}{2}|111\rangle. \end{aligned} \tag{18}$$

After obtaining partial state information through the WM, the feed-forward operators f_0 and f_1 are applied to qubits 2 and 3, respectively, which enable improved robustness. We define

$$f_0 = I = \begin{bmatrix} 1 & 0 \\ 0 & 1 \end{bmatrix}, \; f_1 = \sigma_x = \begin{bmatrix} 0 & 1 \\ 1 & 0 \end{bmatrix}. \tag{19}$$

If the measurement result is m_0, it means that this single-qubit state is close to the ground state and is less affected by noise. Hence, the feed-forward operator f_0 is chosen as the identity matrix. If the measurement result is m_1, it means that this single-qubit state is close to the excited state and is more susceptible to noise interference. Hence,

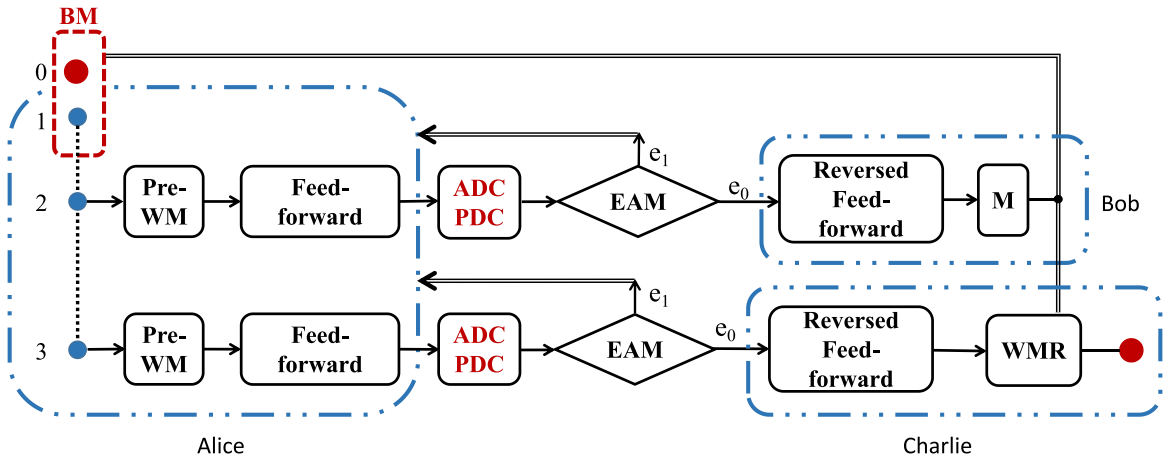

Fig. 3. FF-EM tripartite quantum teleportation protocol. The dashed lines in the figure indicate quantum entanglement, double lines indicate the classical channels, the single lines indicate quantum channels, BM denotes Bell basis measurement, and M denotes the quantum measurement.

the feed-forward operator f_1 is designed as the bit-flip Pauli operator σ_x to make the state transfer towards the ground state.

For the tripartite entangled state, the feed-forward control operators are constructed as

$$\begin{aligned} &F_{00} = I \otimes f_0 \otimes f_0,\ F_{01} = I \otimes f_0 \otimes f_1, \\ &F_{10} = I \otimes f_1 \otimes f_0,\ F_{11} = I \otimes f_1 \otimes f_1. \end{aligned} \tag{20}$$

After employing the feed-forward control operator, the tripartite entangled state becomes $\rho_{F_{ij}} = |\psi_{F_{ij}}\rangle\langle\psi_{F_{ij}}|$ with a probability of $g_{F_{ij}} = \mathrm{Tr}\left(F_{ij}M_{ij}|\psi_{123}\rangle\langle\psi_{123}|M_{ij}^{\dagger}F_{ij}\right)$ and $\sum_{i,j=0,1} g_{F_{ij}} = 1$, where

$$\begin{aligned} |\psi_{F_{00}}\rangle &= \cos\frac{\theta}{2}\cos^2\frac{\omega}{2}|000\rangle + \sin\frac{\theta}{2}\sin^2\frac{\omega}{2}|111\rangle, \\ |\psi_{F_{01}}\rangle &= \cos\frac{\theta}{2}\sin\frac{\omega}{2}\cos\frac{\omega}{2}|001\rangle + \sin\frac{\theta}{2}\sin\frac{\omega}{2}\cos\frac{\omega}{2}|110\rangle, \\ |\psi_{F_{10}}\rangle &= \cos\frac{\theta}{2}\sin\frac{\omega}{2}\cos\frac{\omega}{2}|010\rangle + \sin\frac{\theta}{2}\sin\frac{\omega}{2}\cos\frac{\omega}{2}|101\rangle, \\ |\psi_{F_{11}}\rangle &= \cos\frac{\theta}{2}\sin^2\frac{\omega}{2}|011\rangle + \sin\frac{\theta}{2}\cos^2\frac{\omega}{2}|100\rangle. \end{aligned} \tag{21}$$

• EAM

Qubits 2 and 3 enter the noise channel and we assume that the characteristics of the noise are completely known. For ease of presentation, we only analyze AD and PD noise, whose Kraus operators are given by Eqs. (1) and (2), respectively.

In either case of AD or PD noise, there are no unitary matrices U_0 and U_1 such that Kraus operators e_0 and e_1 satisfy $e_0 = c_0U_0$ and $e_1 = c_1U_1$ (where c_0 and c_1 are constants). Therefore, the EAEC scheme is not applicable. Instead, we employ the EAM scheme, which involves applying measurement operators to the noise environment, causing it to collapse onto an observable eigenstate. As a result, the state of the quantum system coupled with the environment is projected onto a state related to this eigenstate. If the environment state collapses onto the kth eigenstate, for the single-qubit quantum system ρ_0, it will accordingly be at $\rho^k = e_k\rho_0e_k^{\dagger}/\mathrm{Tr}\left(e_k\rho_0e_k^{\dagger}\right)$, where e_k is the reversible Kraus operator.

The entanglement distribution is successful only when the environment measurement result is reversible, otherwise the process is restarted, which makes the protocol a probabilistic scheme. Note that reversible Kraus operators for both AD and PD noise are denoted as $e_0 = |0\rangle\langle 0| + \sqrt{1-r}|1\rangle\langle 1|$. Therefore, the Kraus operator of the noise channel is $E = I \otimes e_0 \otimes e_0$, all other cases containing e_1 are discarded.

After employing the EAM, the tripartite entangled state becomes $\rho_{EF_{ij}} = |\psi_{EF_{ij}}\rangle\langle\psi_{EF_{ij}}|$, where

$$\begin{aligned} |\psi_{EF_{00}}\rangle &= \cos\frac{\theta}{2}\cos^2\frac{\omega}{2}|000\rangle + (1-r)\sin\frac{\theta}{2}\sin^2\frac{\omega}{2}|111\rangle, \\ |\psi_{EF_{01}}\rangle &= \sqrt{1-r}\cos\frac{\theta}{2}\sin\frac{\omega}{2}\cos\frac{\omega}{2}|001\rangle \\ &\quad + \sqrt{1-r}\sin\frac{\theta}{2}\sin\frac{\omega}{2}\cos\frac{\omega}{2}|110\rangle, \\ |\psi_{EF_{10}}\rangle &= \sqrt{1-r}\cos\frac{\theta}{2}\sin\frac{\omega}{2}\cos\frac{\omega}{2}|010\rangle \\ &\quad + \sqrt{1-r}\sin\frac{\theta}{2}\sin\frac{\omega}{2}\cos\frac{\omega}{2}|101\rangle, \\ |\psi_{EF_{11}}\rangle &= (1-r)\cos\frac{\theta}{2}\sin^2\frac{\omega}{2}|011\rangle + \sin\frac{\theta}{2}\cos^2\frac{\omega}{2}|100\rangle. \end{aligned} \tag{22}$$

In this way, the successful probability of EAM is

$$\begin{aligned} g_{EF_{ij}} &= tr\left(EF_{ij}M_{ij}|\psi_{123}\rangle\langle\psi_{123}|M_{ij}^{\dagger}F_{ij}^{\dagger}E^{\dagger}\right), \\ g_{EF} &= \sum_{i,j=0,1} g_{EF_{ij}} = \left(r\sin^2\frac{\omega}{2} - 1\right)^2, \end{aligned} \tag{23}$$

which reaches its maximum value at $\omega = \pi/2$. The maximum value is $g_{EF}^{(opt)} = (1-r/2)^2$.

• Feed-forward reversal

Bob and Charlie receive qubits 2 and 3, respectively. Based on m_i in the last step, Bob and Charlie apply the feed-forward reversal operator f_i^{-1} to qubits to 2 and 3 separately. Since f_i is the unitary matrix given by Eq. (19), we have $\left(f_i \otimes f_j\right)^{-1} = f_i^{-1} \otimes f_j^{-1} = f_i \otimes f_j$, $(j = 0, 1)$. The quantum state then becomes $\rho_{EM_{ij}} = |\psi_{EM_{ij}}\rangle\langle\psi_{EM_{ij}}|$, where

$$\begin{aligned} |\psi_{EM_{00}}\rangle &= \cos\frac{\theta}{2}\cos^2\frac{\omega}{2}|000\rangle + (1-r)\sin\frac{\theta}{2}\sin^2\frac{\omega}{2}|111\rangle, \\ |\psi_{EM_{01}}\rangle &= |\psi_{EM_{10}}\rangle = \sqrt{1-r}\cos\frac{\theta}{2}\sin\frac{\omega}{2}\cos\frac{\omega}{2}|000\rangle \\ &\quad + \sqrt{1-r}\sin\frac{\theta}{2}\sin\frac{\omega}{2}\cos\frac{\omega}{2}|111\rangle, \\ |\psi_{EM_{11}}\rangle &= (1-r)\cos\frac{\theta}{2}\sin^2\frac{\omega}{2}|000\rangle + \sin\frac{\theta}{2}\cos^2\frac{\omega}{2}|111\rangle. \end{aligned} \tag{24}$$

Step 2 Alice performs a joint measurement on qubits 0 and 1, and Bob measures his qubit 2. Since there are four pre-WM operators M_{ij}, it is necessary to discuss the four cases separately. The detailed procedures for the case of M_{00} are given below, which can also be applied to the other cases, and for brevity the other detailed procedures are omitted.

$$\rho_{out_{000}}^{EM_{00}} = \frac{R_{000}^{EM_{00}} \rho_{000}^{EM_{00}} \left(R_{000}^{EM_{00}}\right)^{\dagger}}{\mathrm{Tr}\left(R_{000}^{EM_{00}} \rho_{000}^{EM_{00}} \left(R_{000}^{EM_{00}}\right)^{\dagger}\right)} = \frac{\left((1-r)^2 \sin^2\frac{\theta}{2}\sin^4\frac{\omega}{2}\cos^2\frac{\varphi}{2}\right) \times 2\left((r-1)^2 \sin^2\frac{\theta}{2}\sin^4\frac{\omega}{2} + \cos^2\frac{\theta}{2}\cos^4\frac{\omega}{2}\right)}{2\left(\cos^2\frac{\theta}{2}\cos^4\frac{\omega}{2} + (1-r)^2\sin^2\frac{\theta}{2}\sin^4\frac{\omega}{2}\right) \times \left((1-r)^2\sin^2\frac{\theta}{2}\sin^4\frac{\omega}{2}\cos^2\frac{\varphi}{2}\right)} \times \rho_{in} = \rho_{in} \tag{28}$$

Box I.

Table 2
Bob and Charlie's state $|\eta_{mn}^{EM_{00}}\rangle_{23}$ corresponding to Alice's measurement results $(m,n)_{01}$.

$(m,n)_{01}$	$\lvert\eta_{mn}^{EM_{00}}\rangle_{23}$
(0, 0)	$\lvert\eta_{00}^{EM_{00}}\rangle = \frac{1}{\sqrt{2}N^{EM_{00}}}\left(\alpha\cos\frac{\theta}{2}\cos^2\frac{\omega}{2}\lvert 00\rangle_{23} + \beta(1-r)\sin\frac{\theta}{2}\sin^2\frac{\omega}{2}\lvert 11\rangle_{23}\right)$
(0, 1)	$\lvert\eta_{01}^{EM_{00}}\rangle = \frac{1}{\sqrt{2}N^{EM_{00}}}\left(\beta\cos\frac{\theta}{2}\cos^2\frac{\omega}{2}\lvert 00\rangle_{23} + \alpha(1-r)\sin\frac{\theta}{2}\sin^2\frac{\omega}{2}\lvert 11\rangle_{23}\right)$
(1, 0)	$\lvert\eta_{10}^{EM_{00}}\rangle = \frac{1}{\sqrt{2}N^{EM_{00}}}\left(\alpha\cos\frac{\theta}{2}\cos^2\frac{\omega}{2}\lvert 00\rangle_{23} - \beta(1-r)\sin\frac{\theta}{2}\sin^2\frac{\omega}{2}\lvert 11\rangle_{23}\right)$
(1, 1)	$\lvert\eta_{11}^{EM_{00}}\rangle = \frac{1}{\sqrt{2}N^{EM_{00}}}\left(-\beta\cos\frac{\theta}{2}\cos^2\frac{\omega}{2}\lvert 00\rangle_{23} + \alpha(1-r)\sin\frac{\theta}{2}\sin^2\frac{\omega}{2}\lvert 11\rangle_{23}\right)$

The quantum channel between the tripartite is successfully established with the shared entangled state of

$$|\psi\rangle_{123}^{EM_{00}} = \frac{1}{N^{EM_{00}}}\left(\cos\frac{\theta}{2}\cos^2\frac{\omega}{2}|000\rangle + (1-r)\sin\frac{\theta}{2}\sin^2\frac{\omega}{2}|111\rangle\right), \tag{25}$$

where $N^{EM_{00}} = \sqrt{\cos^2\frac{\theta}{2}\cos^4\frac{\omega}{2} + (1-r)^2\sin^2\frac{\theta}{2}\sin^4\frac{\omega}{2}}$ is the normalized factor.

After using the joint measurement on qubits 0 and 1, Alice's result is $(m,n)_{01}$, and the corresponding qubits 2 and 3 shared by Bob and Charlie are $|\eta_{mn}^{EM_{00}}\rangle_{23}$ given in Table 2.

Bob performs the projective measurement on the qubit 2 using the measurement basis given by Eq. (9), with the measurement result $(k)_2$. In each of the four cases (M_{00}, M_{01}, M_{10}, M_{11}), based on the measurement results $(m,n,k)_{012}$, the state of the qubit 3 $|\psi_{mnk}\rangle_3$ held by Charlie can be determined (given in Tables 3 and 4).

Step 3 Charlie designs and applies the WMR operator to the qubit 3. Based on the measurements, the qubit 3 is reconstructed as the input qubit $|\psi_0\rangle$. For M_{00}, if the measurement results are $(0,0,0)_{012}$, then the state of the qubit 3 is

$$\rho_{000}^{EM_{00}} = |\psi_{000}^{EM_{00}}\rangle\langle\psi_{000}^{EM_{00}}|, \tag{26}$$

where $|\psi_{000}^{EM_{00}}\rangle$ is given in Table 3. To make the final output state as close as possible to the input state, the WMR operator is designed as

$$R_{000}^{EM_{00}} = (1-r)\tan\frac{\theta}{2}\tan^2\frac{\omega}{2}\cot\frac{\varphi}{2}|0\rangle\langle 0| + |1\rangle\langle 1|. \tag{27}$$

Accordingly, the final output state of the qubit 3 can be obtained as Eq. (28) (see Box I).

The WMR operators $R_{mnk}^{EM_{ij}}$ for the four cases M_{00}, M_{01}, M_{10}, M_{11} are obtained analogously, given in Table 5, respectively. The relationship between the initial input state and the final output state can be described by a completely positive and trace-preserving (CPTP) map. Then the normalized output state $\rho_{out_{mnk}}^{EM_{ij}}$ can be given by

$$\rho_{out_{mnk}}^{EM_{ij}} = \frac{R_{mnk}^{EM_{ij}} F_{ij} E F_{ij} M_{ij} |\psi_{123}\rangle\langle\psi_{123}| M_{ij}^{\dagger} F_{ij}^{\dagger} E^{\dagger} F_{ij}^{\dagger} \left(R_{mnk}^{EM_{ij}}\right)^{\dagger}}{\mathrm{Tr}\left(R_{mnk}^{EM_{ij}} F_{ij} E F_{ij} M_{ij} |\psi_{123}\rangle\langle\psi_{123}| M_{ij}^{\dagger} F_{ij}^{\dagger} F_{ij}^{\dagger} \left(R_{mnk}^{EM_{ij}}\right)^{\dagger}\right)} = \frac{R_{mnk}^{EM_{ij}} \rho_{mnk}^{EM_{ij}} \left(R_{mnk}^{EM_{ij}}\right)^{\dagger}}{\mathrm{Tr}\left(R_{mnk}^{EM_{ij}} \rho_{mnk}^{EM_{ij}} \left(R_{mnk}^{EM_{ij}}\right)^{\dagger}\right)}, \tag{29}$$

where $\rho_{mnk}^{EM_{ij}} = |\psi_{mnk}^{EM_{ij}}\rangle\langle\psi_{mnk}^{EM_{ij}}|$, $|\psi_{mnk}^{EM_{ij}}\rangle$ is given in Tables 3 and 4. This verifies that in all cases, the final output state $\rho_{out_{mnk}}^{EM_{ij}}$ is the same as the input state ρ_{in}.

After introducing the process of FF-EM protocol, we use the average fidelity and the total success probability to evaluate the effectiveness. When the measurement results are (m,n,k), the fidelity for M_{ij} is

$$\mathrm{fid}_{mnk}^{EM_{ij}} = \langle\psi_0|\rho_{out_{mnk}}^{EM_{ij}}|\psi_0\rangle = 1. \tag{30}$$

Therefore, the overall average teleportation fidelity is

$$\mathrm{Fid}_{\mathrm{av}}^{\mathrm{FF-EM}} = \int \mathrm{d}\psi \sum_{i,j}\left(\sum_{m,n,k} p_{mnk}^{ij}\,\mathrm{fid}_{mnk}^{ij}\right) = \int \mathrm{d}\psi \sum_{i,j}\sum_{m,n,k} p_{mnk}^{ij} = 1, \tag{31}$$

where p_{mnk}^{ij} is the probability of the measurement results (m,n,k) for M_{ij}, and $\sum_{i,j}\sum_{m,n,k} p_{mnk}^{ij} = 1$. It is worth noting that the fidelity of the protocol proposed in this paper is always equal to 1, i.e., it is not affected by the entanglement angle θ and the magnitude of decoherence r, and the final output state always remains identical to the initial input state.

Since the WMR operator is incomplete, this quantum teleportation protocol is a probabilistic scheme. The success probability for the output state $\rho_{out_{mnk}}^{EM_{ij}}$ is

$$g_{m,n,k}^{EM_{ij}} = \langle\psi_{m,n,k}^{EM_{ij}}| R_{m,n,k}^{EM_{ij}\dagger} R_{m,n,k}^{EM_{ij}} |\psi_{m,n,k}^{EM_{ij}}\rangle \tag{32}$$

with the results given by

$$\begin{aligned}
g_{000}^{EM_{00}} &= g_{010}^{EM_{00}} = g_{100}^{EM_{00}} = g_{110}^{EM_{00}} = \frac{(1-r)^2\sin^2\frac{\theta}{2}\sin^4\frac{\omega}{2}\cos^2\frac{\varphi}{2}}{2\left[(1-r)^2\sin^2\frac{\theta}{2} + \cos^2\frac{\theta}{2}\cos^4\frac{\omega}{2}\right]},\\
g_{001}^{EM_{00}} &= g_{011}^{EM_{00}} = g_{101}^{EM_{00}} = g_{111}^{EM_{00}} = \frac{(1-r)^2\sin^2\frac{\theta}{2}\sin^4\frac{\omega}{2}\sin^2\frac{\varphi}{2}}{2\left[(1-r)^2\sin^2\frac{\theta}{2} + \cos^2\frac{\theta}{2}\cos^4\frac{\omega}{2}\right]},\\
g_{000}^{EM_{01}} &= g_{010}^{EM_{01}} = g_{100}^{EM_{01}} = g_{110}^{EM_{01}} = g_{000}^{EM_{10}} = g_{010}^{EM_{10}} = g_{100}^{EM_{10}}\\
&= g_{110}^{EM_{10}} = \frac{\sin^2\frac{\theta}{2}\cos^2\frac{\varphi}{2}}{2},\\
g_{001}^{EM_{01}} &= g_{011}^{EM_{01}} = g_{101}^{EM_{01}} = g_{111}^{EM_{01}} = g_{001}^{EM_{10}} = g_{011}^{EM_{10}} = g_{101}^{EM_{10}}\\
&= g_{111}^{EM_{10}} = \frac{\sin^2\frac{\theta}{2}\sin^2\frac{\varphi}{2}}{2},\\
g_{000}^{EM_{11}} &= g_{010}^{EM_{11}} = g_{100}^{EM_{11}} = g_{110}^{EM_{11}} = \frac{\sin^2\frac{\theta}{2}\cos^4\frac{\omega}{2}\cos^2\frac{\varphi}{2}}{2\left[(1-r)^2\cos^2\frac{\theta}{2}\sin^4\frac{\omega}{2} + \sin^2\frac{\theta}{2}\cos^4\frac{\omega}{2}\right]},\\
g_{001}^{EM_{11}} &= g_{011}^{EM_{11}} = g_{101}^{EM_{11}} = g_{111}^{EM_{11}} = \frac{\sin^2\frac{\theta}{2}\cos^4\frac{\omega}{2}\sin^2\frac{\varphi}{2}}{2\left[(1-r)^2\cos^2\frac{\theta}{2}\sin^4\frac{\omega}{2} + \sin^2\frac{\theta}{2}\cos^4\frac{\omega}{2}\right]}.
\end{aligned} \tag{33}$$

Table 3
Charlie's states $|\psi_{mnk}^{EM_{ij}}\rangle$ corresponding to the measurement results of Alice and Bob (m,n,k) for M_{00} and M_{01}.

$(m,n,k)_{012}$	$\|\psi_{mnk}^{EM_{00}}\rangle_3$	$\|\psi_{mnk}^{EM_{01}}\rangle_3$
(0,0,0)	$\frac{1}{\sqrt{2}N^{EM_{00}}}\left(\alpha\cos\frac{\theta}{2}\cos^2\frac{\omega}{2}\sin\frac{\varphi}{2}\|0\rangle_3+\beta(1-r)\sin\frac{\theta}{2}\sin^2\frac{\omega}{2}\cos\frac{\varphi}{2}\|1\rangle_3\right)$	$\frac{\sqrt{1-r}\sin\frac{\omega}{2}\cos\frac{\omega}{2}}{\sqrt{2}N^{EM_{01}}}\left(\alpha\cos\frac{\theta}{2}\sin\frac{\varphi}{2}\|0\rangle_3+\beta\sin\frac{\theta}{2}\cos\frac{\varphi}{2}\|1\rangle_3\right)$
(0,0,1)	$\frac{1}{\sqrt{2}N^{EM_{00}}}\left(\alpha\cos\frac{\theta}{2}\cos^2\frac{\omega}{2}\cos\frac{\varphi}{2}\|0\rangle_3-\beta(1-r)\sin\frac{\theta}{2}\sin^2\frac{\omega}{2}\sin\frac{\varphi}{2}\|1\rangle_3\right)$	$\frac{\sqrt{1-r}\sin\frac{\omega}{2}\cos\frac{\omega}{2}}{\sqrt{2}N^{EM_{01}}}\left(\alpha\cos\frac{\theta}{2}\cos\frac{\varphi}{2}\|0\rangle_3-\beta\sin\frac{\theta}{2}\sin\frac{\varphi}{2}\|1\rangle_3\right)$
(0,1,0)	$\frac{1}{\sqrt{2}N^{EM_{00}}}\left(\beta\cos\frac{\theta}{2}\cos^2\frac{\omega}{2}\sin\frac{\varphi}{2}\|0\rangle_3+\alpha(1-r)\sin\frac{\theta}{2}\sin^2\frac{\omega}{2}\cos\frac{\varphi}{2}\|1\rangle_3\right)$	$\frac{\sqrt{1-r}\sin\frac{\omega}{2}\cos\frac{\omega}{2}}{\sqrt{2}N^{EM_{01}}}\left(\beta\cos\frac{\theta}{2}\sin\frac{\varphi}{2}\|0\rangle_3+\alpha\sin\frac{\theta}{2}\cos\frac{\varphi}{2}\|1\rangle_3\right)$
(0,0,1)	$\frac{1}{\sqrt{2}N^{EM_{00}}}\left(\beta\cos\frac{\theta}{2}\cos^2\frac{\omega}{2}\cos\frac{\varphi}{2}\|0\rangle_3-\alpha(1-r)\sin\frac{\theta}{2}\sin^2\frac{\omega}{2}\sin\frac{\varphi}{2}\|1\rangle_3\right)$	$\frac{\sqrt{1-r}\sin\frac{\omega}{2}\cos\frac{\omega}{2}}{\sqrt{2}N^{EM_{01}}}\left(\beta\cos\frac{\theta}{2}\cos\frac{\varphi}{2}\|0\rangle_3-\alpha\sin\frac{\theta}{2}\sin\frac{\varphi}{2}\|1\rangle_3\right)$
(1,0,0)	$\frac{1}{\sqrt{2}N^{EM_{00}}}\left(\alpha\cos\frac{\theta}{2}\cos^2\frac{\omega}{2}\sin\frac{\varphi}{2}\|0\rangle_3-\beta(1-r)\sin\frac{\theta}{2}\sin^2\frac{\omega}{2}\cos\frac{\varphi}{2}\|1\rangle_3\right)$	$\frac{\sqrt{1-r}\sin\frac{\omega}{2}\cos\frac{\omega}{2}}{\sqrt{2}N^{EM_{01}}}\left(\alpha\cos\frac{\theta}{2}\sin\frac{\varphi}{2}\|0\rangle_3-\beta\sin\frac{\theta}{2}\cos\frac{\varphi}{2}\|1\rangle_3\right)$
(1,0,1)	$\frac{1}{\sqrt{2}N^{EM_{00}}}\left(\alpha\cos\frac{\theta}{2}\cos^2\frac{\omega}{2}\cos\frac{\varphi}{2}\|0\rangle_3+\beta(1-r)\sin\frac{\theta}{2}\sin^2\frac{\omega}{2}\sin\frac{\varphi}{2}\|1\rangle_3\right)$	$\frac{\sqrt{1-r}\sin\frac{\omega}{2}\cos\frac{\omega}{2}}{\sqrt{2}N^{EM_{01}}}\left(\alpha\cos\frac{\theta}{2}\cos\frac{\varphi}{2}\|0\rangle_3+\beta\sin\frac{\theta}{2}\sin\frac{\varphi}{2}\|1\rangle_3\right)$
(1,1,0)	$\frac{1}{\sqrt{2}N^{EM_{00}}}\left(-\beta\cos\frac{\theta}{2}\cos^2\frac{\omega}{2}\sin\frac{\varphi}{2}\|0\rangle_3+\alpha(1-r)\sin\frac{\theta}{2}\sin^2\frac{\omega}{2}\cos\frac{\varphi}{2}\|1\rangle_3\right)$	$\frac{\sqrt{1-r}\sin\frac{\omega}{2}\cos\frac{\omega}{2}}{\sqrt{2}N^{EM_{01}}}\left(-\beta\cos\frac{\theta}{2}\sin\frac{\varphi}{2}\|0\rangle_3+\alpha\sin\frac{\theta}{2}\cos\frac{\varphi}{2}\|1\rangle_3\right)$
(1,1,1)	$\frac{1}{\sqrt{2}N^{EM_{00}}}\left(-\beta\cos\frac{\theta}{2}\cos^2\frac{\omega}{2}\cos\frac{\varphi}{2}\|0\rangle_3-\alpha(1-r)\sin\frac{\theta}{2}\sin^2\frac{\omega}{2}\sin\frac{\varphi}{2}\|1\rangle_3\right)$	$\frac{\sqrt{1-r}\sin\frac{\omega}{2}\cos\frac{\omega}{2}}{\sqrt{2}N^{EM_{01}}}\left(-\beta\cos\frac{\theta}{2}\cos\frac{\varphi}{2}\|0\rangle_3-\alpha\sin\frac{\theta}{2}\sin\frac{\varphi}{2}\|1\rangle_3\right)$

Table 4
Charlie's states $|\psi_{mnk}^{EM_{ij}}\rangle$ corresponding to the measurement results of Alice and Bob (m,n,k) for M_{10} and M_{11}.

$(m,n,k)_{012}$	$\|\psi_{mnk}^{EM_{10}}\rangle_3$	$\|\psi_{mnk}^{EM_{11}}\rangle_3$
(0,0,0)	$\frac{\sqrt{1-r}\sin\frac{\omega}{2}\cos\frac{\omega}{2}}{\sqrt{2}N^{EM_{10}}}\left(\alpha\cos\frac{\theta}{2}\sin\frac{\varphi}{2}\|0\rangle_3+\beta\sin\frac{\theta}{2}\cos\frac{\varphi}{2}\|1\rangle_3\right)$	$\frac{1}{\sqrt{2}N^{EM_{11}}}\left(\alpha(1-r)\cos\frac{\theta}{2}\sin^2\frac{\omega}{2}\sin\frac{\varphi}{2}\|0\rangle_3+\beta\sin\frac{\theta}{2}\cos^2\frac{\omega}{2}\cos\frac{\varphi}{2}\|1\rangle_3\right)$
(0,0,1)	$\frac{\sqrt{1-r}\sin\frac{\omega}{2}\cos\frac{\omega}{2}}{\sqrt{2}N^{EM_{10}}}\left(\alpha\cos\frac{\theta}{2}\cos\frac{\varphi}{2}\|0\rangle_3-\beta\sin\frac{\theta}{2}\sin\frac{\varphi}{2}\|1\rangle_3\right)$	$\frac{1}{\sqrt{2}N^{EM_{11}}}\left(\alpha(1-r)\cos\frac{\theta}{2}\sin^2\frac{\omega}{2}\cos\frac{\varphi}{2}\|0\rangle_3-\beta\sin\frac{\theta}{2}\cos^2\frac{\omega}{2}\sin\frac{\varphi}{2}\|1\rangle_3\right)$
(0,1,0)	$\frac{\sqrt{1-r}\sin\frac{\omega}{2}\cos\frac{\omega}{2}}{\sqrt{2}N^{EM_{10}}}\left(\beta\cos\frac{\theta}{2}\sin\frac{\varphi}{2}\|0\rangle_3+\alpha\sin\frac{\theta}{2}\cos\frac{\varphi}{2}\|1\rangle_3\right)$	$\frac{1}{\sqrt{2}N^{EM_{11}}}\left(\beta(1-r)\cos\frac{\theta}{2}\sin^2\frac{\omega}{2}\sin\frac{\varphi}{2}\|0\rangle_3+\alpha\sin\frac{\theta}{2}\cos^2\frac{\omega}{2}\cos\frac{\varphi}{2}\|1\rangle_3\right)$
(0,0,1)	$\frac{\sqrt{1-r}\sin\frac{\omega}{2}\cos\frac{\omega}{2}}{\sqrt{2}N^{EM_{10}}}\left(\beta\cos\frac{\theta}{2}\cos\frac{\varphi}{2}\|0\rangle_3-\alpha\sin\frac{\theta}{2}\sin\frac{\varphi}{2}\|1\rangle_3\right)$	$\frac{1}{\sqrt{2}N^{EM_{11}}}\left(\beta(1-r)\cos\frac{\theta}{2}\sin^2\frac{\omega}{2}\cos\frac{\varphi}{2}\|0\rangle_3-\alpha\sin\frac{\theta}{2}\cos^2\frac{\omega}{2}\sin\frac{\varphi}{2}\|1\rangle_3\right)$
(1,0,0)	$\frac{\sqrt{1-r}\sin\frac{\omega}{2}\cos\frac{\omega}{2}}{\sqrt{2}N^{EM_{10}}}\left(\alpha\cos\frac{\theta}{2}\sin\frac{\varphi}{2}\|0\rangle_3-\beta\sin\frac{\theta}{2}\cos\frac{\varphi}{2}\|1\rangle_3\right)$	$\frac{1}{\sqrt{2}N^{EM_{11}}}\left(\alpha(1-r)\cos\frac{\theta}{2}\sin^2\frac{\omega}{2}\sin\frac{\varphi}{2}\|0\rangle_3-\beta\sin\frac{\theta}{2}\cos^2\frac{\omega}{2}\cos\frac{\varphi}{2}\|1\rangle_3\right)$
(1,0,1)	$\frac{\sqrt{1-r}\sin\frac{\omega}{2}\cos\frac{\omega}{2}}{\sqrt{2}N^{EM_{10}}}\left(\alpha\cos\frac{\theta}{2}\cos\frac{\varphi}{2}\|0\rangle_3+\beta\sin\frac{\theta}{2}\sin\frac{\varphi}{2}\|1\rangle_3\right)$	$\frac{1}{\sqrt{2}N^{EM_{11}}}\left(\alpha(1-r)\cos\frac{\theta}{2}\sin^2\frac{\omega}{2}\cos\frac{\varphi}{2}\|0\rangle_3+\beta\sin\frac{\theta}{2}\cos^2\frac{\omega}{2}\sin\frac{\varphi}{2}\|1\rangle_3\right)$
(1,1,0)	$\frac{\sqrt{1-r}\sin\frac{\omega}{2}\cos\frac{\omega}{2}}{\sqrt{2}N^{EM_{10}}}\left(-\beta\cos\frac{\theta}{2}\sin\frac{\varphi}{2}\|0\rangle_3+\alpha\sin\frac{\theta}{2}\cos\frac{\varphi}{2}\|1\rangle_3\right)$	$\frac{1}{\sqrt{2}N^{EM_{11}}}\left(-\beta(1-r)\cos\frac{\theta}{2}\sin^2\frac{\omega}{2}\sin\frac{\varphi}{2}\|0\rangle_3+\alpha\sin\frac{\theta}{2}\cos^2\frac{\omega}{2}\cos\frac{\varphi}{2}\|1\rangle_3\right)$
(1,1,1)	$\frac{\sqrt{1-r}\sin\frac{\omega}{2}\cos\frac{\omega}{2}}{\sqrt{2}N^{EM_{10}}}\left(-\beta\cos\frac{\theta}{2}\cos\frac{\varphi}{2}\|0\rangle_3-\alpha\sin\frac{\theta}{2}\sin\frac{\varphi}{2}\|1\rangle_3\right)$	$\frac{1}{\sqrt{2}N^{EM_{11}}}\left(-\beta(1-r)\cos\frac{\theta}{2}\sin^2\frac{\omega}{2}\cos\frac{\varphi}{2}\|0\rangle_3-\alpha\sin\frac{\theta}{2}\cos^2\frac{\omega}{2}\sin\frac{\varphi}{2}\|1\rangle_3\right)$

Table 5
WMR operators $R_{mnk}^{EM_{ij}}$ used by Charlie corresponding to the measurement results of Alice and Bob (m,n,k).

$(m,n,k)_{012}$	$R_{mnk}^{EM_{00}}$	$R_{mnk}^{EM_{01,10}}$	$R_{mnk}^{EM_{11}}$
(0,0,0)	$(1-r)\tan\frac{\theta}{2}\tan^2\frac{\omega}{2}\cot\frac{\varphi}{2}\|0\rangle\langle0\|+\|1\rangle\langle1\|$	$\tan\frac{\theta}{2}\cot\frac{\varphi}{2}\|0\rangle\langle0\|+\|1\rangle\langle1\|$	$\frac{1}{1-r}\tan\frac{\theta}{2}\cot^2\frac{\omega}{2}\cot\frac{\varphi}{2}\|0\rangle\langle0\|+\|1\rangle\langle1\|$
(0,0,1)	$\sigma_z\left[(1-r)\tan\frac{\theta}{2}\tan^2\frac{\omega}{2}\tan\frac{\varphi}{2}\|0\rangle\langle0\|+\|1\rangle\langle1\|\right]$	$\sigma_z\left(\tan\frac{\theta}{2}\tan\frac{\varphi}{2}\|0\rangle\langle0\|+\|1\rangle\langle1\|\right)$	$\sigma_z\left[\frac{1}{1-r}\tan\frac{\theta}{2}\cot^2\frac{\omega}{2}\tan\frac{\varphi}{2}\|0\rangle\langle0\|+\|1\rangle\langle1\|\right]$
(0,1,0)	$\sigma_x\left[(1-r)\tan\frac{\theta}{2}\tan^2\frac{\omega}{2}\cot\frac{\varphi}{2}\|0\rangle\langle0\|+\|1\rangle\langle1\|\right]$	$\sigma_x\left(\tan\frac{\theta}{2}\cot\frac{\varphi}{2}\|0\rangle\langle0\|+\|1\rangle\langle1\|\right)$	$\sigma_x\left[\frac{1}{1-r}\tan\frac{\theta}{2}\cot^2\frac{\omega}{2}\cot\frac{\varphi}{2}\|0\rangle\langle0\|+\|1\rangle\langle1\|\right]$
(0,1,1)	$\sigma_x\sigma_z\left[(1-r)\tan\frac{\theta}{2}\tan^2\frac{\omega}{2}\tan\frac{\varphi}{2}\|0\rangle\langle0\|+\|1\rangle\langle1\|\right]$	$\sigma_x\sigma_z\left(\tan\frac{\theta}{2}\tan\frac{\varphi}{2}\|0\rangle\langle0\|+\|1\rangle\langle1\|\right)$	$\sigma_x\sigma_z\left[\frac{1}{1-r}\tan\frac{\theta}{2}\cot^2\frac{\omega}{2}\tan\frac{\varphi}{2}\|0\rangle\langle0\|+\|1\rangle\langle1\|\right]$
(1,0,0)	$\sigma_z\left((1-r)\tan\frac{\theta}{2}\tan^2\frac{\omega}{2}\cot\frac{\varphi}{2}\|0\rangle\langle0\|+\|1\rangle\langle1\|\right)$	$\sigma_z\left(\tan\frac{\theta}{2}\cot\frac{\varphi}{2}\|0\rangle\langle0\|+\|1\rangle\langle1\|\right)$	$\sigma_z\left[\frac{1}{1-r}\tan\frac{\theta}{2}\cot^2\frac{\omega}{2}\cot\frac{\varphi}{2}\|0\rangle\langle0\|+\|1\rangle\langle1\|\right]$
(1,0,1)	$(1-r)\tan\frac{\theta}{2}\tan^2\frac{\omega}{2}\tan\frac{\varphi}{2}\|0\rangle\langle0\|+\|1\rangle\langle1\|$	$\tan\frac{\theta}{2}\tan\frac{\varphi}{2}\|0\rangle\langle0\|+\|1\rangle\langle1\|$	$\frac{1}{1-r}\tan\frac{\theta}{2}\cot^2\frac{\omega}{2}\tan\frac{\varphi}{2}\|0\rangle\langle0\|+\|1\rangle\langle1\|$
(1,1,0)	$\sigma_x\sigma_z\left[(1-r)\tan\frac{\theta}{2}\tan^2\frac{\omega}{2}\cot\frac{\varphi}{2}\|0\rangle\langle0\|+\|1\rangle\langle1\|\right]$	$\sigma_x\sigma_z\left(\tan\frac{\theta}{2}\cot\frac{\varphi}{2}\|0\rangle\langle0\|+\|1\rangle\langle1\|\right)$	$\sigma_x\sigma_z\left[\frac{1}{1-r}\tan\frac{\theta}{2}\cot^2\frac{\omega}{2}\cot\frac{\varphi}{2}\|0\rangle\langle0\|+\|1\rangle\langle1\|\right]$
(1,0,1)	$\sigma_x\left[(1-r)\tan\frac{\theta}{2}\tan^2\frac{\omega}{2}\tan\frac{\varphi}{2}\|0\rangle\langle0\|+\|1\rangle\langle1\|\right]$	$\sigma_x\left(\tan\frac{\theta}{2}\tan\frac{\varphi}{2}\|0\rangle\langle0\|+\|1\rangle\langle1\|\right)$	$\sigma_x\left[\frac{1}{1-r}\tan\frac{\theta}{2}\cot^2\frac{\omega}{2}\tan\frac{\varphi}{2}\|0\rangle\langle0\|+\|1\rangle\langle1\|\right]$

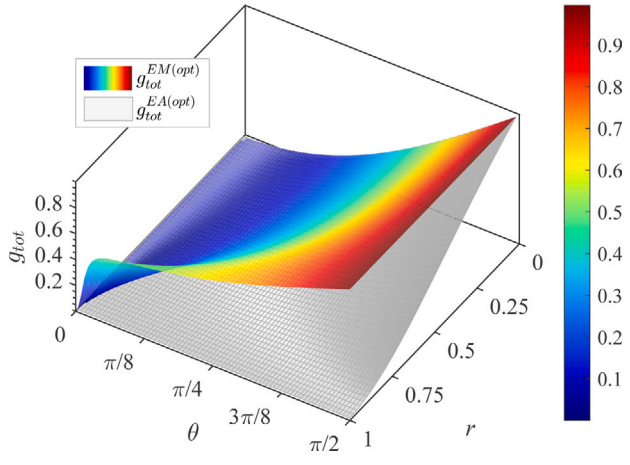

Fig. 4. Success probabilities of FF-EM and EA-WMR protocol with successful EAM.

In this way, the success probability for various cases can be obtained separately as $g_{EM_{ij}}=\sum_{m,n,k} g_{mnk}^{EM_{ij}}$, i.e.,

$$\begin{aligned} g_{EM_{00}} &= \frac{2(1-r)^2\sin^2\frac{\theta}{2}\sin^4\frac{\omega}{2}}{(1-r)^2\sin^2\frac{\theta}{2}+\cos^2\frac{\theta}{2}\cos^4\frac{\omega}{2}}, \\ g_{EM_{01}} &= g_{EM_{10}} = 2\sin^2\frac{\theta}{2}, \\ g_{EM_{11}} &= \frac{2\sin^2\frac{\theta}{2}\cos^4\frac{\omega}{2}}{(1-r)^2\cos^2\frac{\theta}{2}\sin^4\frac{\omega}{2}+\sin^2\frac{\theta}{2}\cos^4\frac{\omega}{2}}, \end{aligned} \tag{34}$$

where $g_{EM_{ij}}$ reaches its maximum value $g_{EM_{ij}}^{(opt)}$ at $\omega=\pi/2$.

Therefore, the total success probability for all cases (M_{00}, M_{01}, M_{10}, M_{11}) is

$$g_{tot}^{EM}=\frac{\sum_{i,j} g_{EM_{ij}}\times g_{M_{ij}}}{\sum_{i,j} g_{M_{ij}}}. \tag{35}$$

To demonstrate the superiority of our protocol, we compare the FF-EM protocol with EA-WMR. Since both two protocols achieve the fidelity of 1, we only need to compare their success probability.

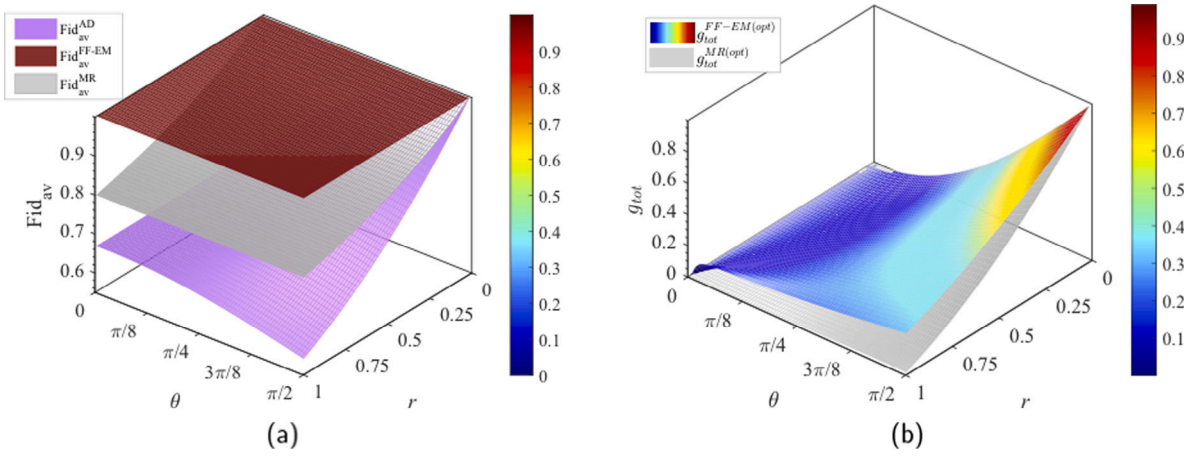

Fig. 5. **(a)** Average teleportation fidelities of FF-EM protocol, MR framework protocol and standard teleportation protocol. Note that the average teleportation fidelity of $\mathrm{Fid}_{av}^{\mathrm{FF-EM}}$ maintains 1, and therefore its surface maintains the deepest color of the colormap. **(b)** Total success probabilities of FF-EM protocol and MR framework protocol. (For interpretation of the references to color in this figure legend, the reader is referred to the web version of this article.)

For FF-EM, the maximum success probability based on successful EAM (i.e., $\omega = \pi/2$) is given by

$$g_{tot}^{EM(opt)} = \frac{\sum_{i,j} g_{EM_{ij}}^{(opt)} \times g_{M_{ij}}}{\sum_{i,j} g_{M_{ij}}} = \sin^2\frac{\theta}{2} + \frac{\sin^2\frac{\theta}{2}}{2\left((1-r)^2\cos^2\frac{\theta}{2} + \sin^2\frac{\theta}{2}\right)} + \frac{(1-r)^2\sin^2\frac{\theta}{2}}{2\left((1-r)^2\sin^2\frac{\theta}{2} + \cos^2\frac{\theta}{2}\right)}. \tag{36}$$

For EA-WMR, the maximum success probability based on successful EAM is [35]

$$g_{tot}^{EA(opt)} = \frac{(1-r)^2\sin^2\frac{\theta}{2}}{(1-r)^2\sin^2\frac{\theta}{2} + \cos^2\frac{\theta}{2}}. \tag{37}$$

Fig. 4 shows the success probabilities of these two protocols. It can be seen that our protocol outperforms EA-WMR in terms of success probability under all entanglement parameters and the magnitude of decoherence. Moreover, our protocol exhibits enhanced robustness against noise as the interference increases. Even at the maximum entanglement (i.e., $\theta = \pi/2$), the success probability of the EA-WMR protocol rapidly decreases as r increases, whereas our protocol remains unaffected by the noise (achieving a success probability of 1).

From Eqs. (23) and (36), g_{EF} and g_{tot}^{EM} both achieve the maximum values at $\omega = \pi/2$. Since the total success probability of our protocol is $g_{tot}^{FF-EM} = g_{tot}^{EM} \times g_{EF}$, when $\omega = \pi/2$, it reaches maximum value $g_{tot}^{FF-EM(opt)}$ shown as

$$g_{tot}^{FF-EM(opt)} = g_{tot}^{EM(opt)} \times g_{EF}^{(opt)} = \left[\sin^2\frac{\theta}{2} + \frac{\sin^2\frac{\theta}{2}}{2\left((1-r)^2\cos^2\frac{\theta}{2} + \sin^2\frac{\theta}{2}\right)} + \frac{(1-r)^2\sin^2\frac{\theta}{2}}{2\left((1-r)^2\sin^2\frac{\theta}{2} + \cos^2\frac{\theta}{2}\right)}\right]\left(1-\frac{r}{2}\right)^2. \tag{38}$$

Furthermore, to highlight the superiority of our FF-EM protocol, we compare it with the teleportation protocol based on WM in the general quantum measurement framework as described in [23]. The optimal average fidelity of the general quantum measurement framework for all possible input states $|\psi_0\rangle$ is

$$\mathrm{Fid}_{\mathrm{av}}^{\mathrm{MR}} = \int \mathrm{d}\psi \left[\frac{1+r|\alpha|^2|\beta|^2}{2\left(1+r|\beta|^2\right)} + \frac{1+r|\alpha|^2|\beta|^2}{2\left(1+r|\alpha|^2\right)}\right], \tag{39}$$

which has a maximum success probability of

$$g_{tot}^{MR(opt)} = 2(1-r)\sin^2\frac{\theta}{2} + r(1-r)\sin^2\frac{\theta}{2}\tan^2\frac{\theta}{2}. \tag{40}$$

Fig. 5(a) shows how the average teleportation fidelities of FF-EM protocol and MR framework protocol change with the magnitude of decoherence r and the entanglement parameter θ. It can be seen that the average fidelity of the MR framework protocol decreases sharply as r increases. However, the average fidelity of the proposed FF-EM protocol is independent of the entanglement parameter and the magnitude of decoherence (constant at 1) and the FF-EM protocol effectively improves the average fidelity in the noise environment. Fig. 5(b) shows how the total success probabilities of the FF-EM protocol, MR framework protocol, and standard teleportation protocol change with the magnitude of decoherence r and the entanglement parameter θ. As r increases, the success probabilities of both protocols decrease, but our proposed FF-EM protocol consistently exhibits higher overall success probabilities compared to the MR framework protocol. It should be noted that the FF-EM protocol is more robust against noise, especially in heavy damping cases ($r \in [0.5, 1]$). When $r = 1$, both the EA-WMR protocol and the MR frame method fail (the success probability is 0), while the FF-EM protocol still has a non-zero success probability.

Overall, our proposed FF-EM protocol outperforms both the MR framework and the EA-WMR protocol in terms of fidelity and success probability, and is more robust against noise, especially under strong decoherence.

Conclusion

This paper proposed a tripartite quantum teleportation protocol with QFFC and EAM, allowing the transmission of arbitrary unknown quantum states through noisy channels. One advantage of the proposed protocol lies in that the average teleportation fidelity is not affected by the entanglement parameters and the magnitude of decoherence. Even using non-maximally entangled states under heavy damping conditions, a high fidelity can still be achieved. In addition, our protocol is suitable for scenarios with both AD and PD. The applicability of QFFC is extended by employing the EAM in the decoherence channel. Numerical results demonstrate that, compared to the standard quantum teleportation protocol, the protocol proposed in this paper effectively improves the average fidelity and success probability of quantum teleportation in the noise environment. In future research, we plan to apply the protocol to multi-node entanglement swapping networks based on quantum teleportation, to address more complex quantum communications in the presence of noise.

Funding

This work was supported by the National Natural Science Foundation of China under Grant 62373342.

CRediT authorship contribution statement

Peiyao Zhang: Conceptualization, Software, Investigation, Formal analysis, Validation, Writing – original draft. **Xiujuan Lu:** Formal analysis, Investigation, Validation, Writing – review & editing. **Sen Kuang:** Validation, Investigation, Supervision, Funding acquisition, Writing – review & editing. **Daoyi Dong:** Supervision, Validation, Writing – review & editing.

Declaration of competing interest

The authors declare that they have no known competing financial interests or personal relationships that could have appeared to influence the work reported in this paper.

Data availability

Data will be made available on request.

References

[1] Sun Q-C, Mao Y-L, Chen S-J, Zhang W, Jiang Y-F, Zhang Y-B, et al. Quantum teleportation with independent sources and prior entanglement distribution over a network. Nat Photonics 2016;10(10):671–5. http://dx.doi.org/10.1038/nphoton.2016.179.

[2] Valivarthi R, Puigibert MlG, Zhou Q, Aguilar GH, Verma VB, Marsili F, et al. Quantum teleportation across a metropolitan fibre network. Nat Photonics 2016;10(10):676–80. http://dx.doi.org/10.1038/nphoton.2016.180.

[3] Ren J-G, Xu P, Yong H-L, Zhang L, Liao S-K, Yin J, et al. Ground-to-satellite quantum teleportation. Nature 2017;549(7670):70–3. http://dx.doi.org/10.1038/nature23675.

[4] Zarmehi F, Houshmand M. Controlled bidirectional quantum secure direct communication network using classical XOR operation and quantum entanglement. IEEE Commun Lett 2016;20(10):2071–4. http://dx.doi.org/10.1109/LCOMM.2016.2589263.

[5] Shang T, Zhao X-J, Liu J-W. Quantum network coding based on controlled teleportation. IEEE Commun Lett 2014;18(5):865–8. http://dx.doi.org/10.1109/LCOMM.2014.033014.132816.

[6] Zarmehi F, Talebi S, Pourkarimi MR. Quantum walk-based controlled quantum teleportation schemes under the effect of decoherence in Markovian and non-Markovian regimes. Quantum Inf Process 2023;22(12):436. http://dx.doi.org/10.1007/s11128-023-04190-z.

[7] Seida C, El Allati A, Metwally N, Hassouni Y. Multi-party bidirectional teleportation. Optik 2021;247:167784. http://dx.doi.org/10.1016/j.ijleo.2021.167784.

[8] Verma V. Bidirectional quantum teleportation by using two GHZ-states as the quantum channel. IEEE Commun Lett 2020;25(3):936–9. http://dx.doi.org/10.1109/LCOMM.2020.3036587.

[9] Zarmehi F, Kochakzadeh MH, Abbasi-Moghadam D, Talebi S. Efficient circular controlled quantum teleportation and broadcast schemes in the presence of quantum noises. Quantum Inf Process 2021;20(5):175. http://dx.doi.org/10.1007/s11128-021-03088-y.

[10] Verma V, Yadav D, Mishra DK. Improvement on cyclic controlled teleportation by using a seven-qubit entangled state. Opt Quantum Electron 2021;53:1–11. http://dx.doi.org/10.1007/s11082-021-03098-1.

[11] Li Z-D, Zhang R, Yin X-F, Liu L-Z, Hu Y, Fang Y-Q, et al. Experimental quantum repeater without quantum memory. Nat Photonics 2019;13(9):644–8. http://dx.doi.org/10.1038/s41566-019-0468-5.

[12] Wang H, Trusheim ME, Kim L, Raniwala H, Englund DR. Field programmable spin arrays for scalable quantum repeaters. Nature Commun 2023;14(1):704. http://dx.doi.org/10.1038/s41467-023-36098-8.

[13] Karlsson A, Bourennane M. Quantum teleportation using three-particle entanglement. Phys Rev A 1998;58(6):4394. http://dx.doi.org/10.1109/EQEC.1998.714867.

[14] Joy D, Sabir M. Efficient schemes for the quantum teleportation of a subclass of tripartite entangled states. Quantum Inf Process 2018;17:1–11. http://dx.doi.org/10.1007/s11128-018-1937-3.

[15] Nielsen MA, Chuang IL. Quantum computation and quantum information. Cambridge University Press; 2010, http://dx.doi.org/10.1017/cbo9780511976667.

[16] Giovannetti V, Lloyd S, Maccone L. Quantum-enhanced measurements: beating the standard quantum limit. Science 2004;306(5700):1330–6. http://dx.doi.org/10.1126/science.1104149.

[17] Dong D, Petersen IR, Rabitz H. Sampled-data design for robust control of a single qubit. IEEE Trans Automat Control 2013;58(10):2654–9. http://dx.doi.org/10.1109/TAC.2013.2256017.

[18] Cramer J, Kalb N, Rol MA, Hensen B, Blok MS, Markham M, et al. Repeated quantum error correction on a continuously encoded qubit by real-time feedback. Nature Commun 2016;7(1):11526. http://dx.doi.org/10.1038/ncomms11526.

[19] Ofek N, Petrenko A, Heeres R, Reinhold P, Leghtas Z, Vlastakis B, et al. Extending the lifetime of a quantum bit with error correction in superconducting circuits. Nature 2016;536(7617):441–5. http://dx.doi.org/10.1038/nature18949.

[20] Pan J-W, Gasparoni S, Ursin R, Weihs G, Zeilinger A. Experimental entanglement purification of arbitrary unknown states. Nature 2003;423(6938):417–22. http://dx.doi.org/10.1038/nature01623.

[21] Zhao Z, Yang T, Chen Y-A, Zhang A-N, Pan J-W. Experimental realization of entanglement concentration and a quantum repeater. Phys Rev Lett 2003;90(20):207901. http://dx.doi.org/10.1103/PhysRevLett.90.207901.

[22] Du J, Rong X, Zhao N, Wang Y, Yang J, Liu R. Preserving electron spin coherence in solids by optimal dynamical decoupling. Nature 2009;461(7268):1265–8. http://dx.doi.org/10.1038/nature08470.

[23] Im D-G, Lee C-H, Kim Y, Nha H, Kim M, Lee S-W, et al. Optimal teleportation via noisy quantum channels without additional qubit resources. npj Quant Inf 2021;7(1):86. http://dx.doi.org/10.1038/s41534-021-00426-x.

[24] Lee S-W, Im D-G, Kim Y-H, Nha H, Kim M. Quantum teleportation is a reversal of quantum measurement. Phys Rev Res 2021;3(3):033119. http://dx.doi.org/10.1103/PhysRevResearch.3.033119.

[25] Harraz S, Cong S, Nieto JJ. Enhancing quantum teleportation fidelity under decoherence via weak measurement with flips. EPJ Quant Technol 2022;9(1):1–12. http://dx.doi.org/10.1140/epjqt/s40507-022-00134-1.

[26] Kim Y-S, Lee J-C, Kwon O, Kim Y-H. Protecting entanglement from decoherence via weak quantum measurement. In: Conference on lasers and electro-optics/Pacific rim. Optica Publishing Group; 2013, p. 1–2. http://dx.doi.org/10.1109/CLEOPR.2013.6600351.

[27] Lee J-C, Jeong Y-C, Kim Y-S, Kim Y-H. Experimental demonstration of decoherence suppression via quantum measurement reversal. Opt Express 2011;19(17):16309–16. http://dx.doi.org/10.1364/OE.19.016309.

[28] Gillett G, Dalton R, Lanyon B, Almeida M, Barbieri M, Pryde GJ, et al. Experimental feedback control of quantum systems using weak measurements. Phys Rev Lett 2010;104(8):080503. http://dx.doi.org/10.1103/PhysRevLett.104.080503.

[29] Yan Y, Zou J, Wang L, Xu B-M, Wang C-Q, Shao B. Quantum state preparation and protection by measurement-based feedback control against decoherence. Commun Theor Phys (Beijing) 2015;63(2):149. http://dx.doi.org/10.1088/0253-6102/63/2/06.

[30] Lim H-T, Lee J-C, Hong K-H, Kim Y-H. Avoiding entanglement sudden death using single-qubit quantum measurement reversal. Opt Express 2014;22(16):19055–68. http://dx.doi.org/10.1364/OE.22.019055.

[31] Harraz S, Cong S. N-qubit state protection against amplitude damping by quantum feed-forward control and its reversal. IEEE J Sel Top Quantum Electron 2020;26(3):1–8. http://dx.doi.org/10.1109/JSTQE.2020.2969574.

[32] Chen Y, Zou J, Long Z-w, Shao B. Protecting quantum Fisher information of N-qubit GHZ state by weak measurement with flips against dissipation. Sci Rep 2017;7(1):6160. http://dx.doi.org/10.1038/s41598-017-04726-1.

[33] Zhao X, Hedemann SR, Yu T. Restoration of a quantum state in a dephasing channel via environment-assisted error correction. Phys Rev A 2013;88(2):022321. http://dx.doi.org/10.1103/PhysRevA.88.022321.

[34] Wang K, Zhao X, Yu T. Environment-assisted quantum state restoration via weak measurements. Phys Rev A 2014;89(4):042320. http://dx.doi.org/10.1103/PhysRevA.89.042320.

[35] Harraz S, Cong S, Nieto JJ. Optimal tripartite quantum teleportation protocol through noisy channels. Quantum Inf Process 2023;22(1):83. http://dx.doi.org/10.1007/s11128-023-03830-8.

[36] Guan S-Y, Jin Z, Wu H-J, Zhu A-D, Wang H-F, Zhang S. Restoration of three-qubit entanglements and protection of tripartite quantum state sharing over noisy channels via environment-assisted measurement and reversal weak measurement. Quantum Inf Process 2017;16:1–15. http://dx.doi.org/10.1007/s11128-017-1584-0.

[37] Harraz S, Zhang J-Y, Cong S. High-fidelity quantum teleportation through noisy channels via weak measurement and environment-assisted measurement. Results Phys 2023;55:107164. http://dx.doi.org/10.1016/j.rinp.2023.107164.